

# Confrontation of QMD model with the experimental data for

$^{40}\text{Ar} + ^{45}\text{Sc}$ ,  $^{197}\text{Au} + ^{197}\text{Au}$  and  $^{129}\text{Xe} + ^{119}\text{Sn}$  reactions

Tajinder Pal Singh<sup>a</sup> and Sakshi Gautam<sup>b 1</sup>

<sup>a</sup>*Handloom street, H.No.-B-9-1076, Surgapuri, Kotkapura (Distt. Faridkot)-151204, India*

<sup>b</sup>*Department of Physics, Panjab University, Chandigarh -160 014, India.*

In the present work, we make confrontation of our theoretical calculations using quantum molecular dynamics model with the experimental data for the reactions of  $^{40}\text{Ar} + ^{45}\text{Sc}$ ,  $^{197}\text{Au} + ^{197}\text{Au}$  and  $^{129}\text{Xe} + ^{119}\text{Sn}$  at different incident energies. In these reactions, we display the charge distribution and energy dependence of fragments multiplicity. Our results indicate good agreement with the experimental data for all the reactions .

---

<sup>1</sup>Email: sakshigautm@gmail.com

# 1 Introduction

Nuclear physics, in general and heavy-ion collisions, in particular, are of central interest due to several rare phenomena emerging at different incident energies. These include (1) collective flow and its disappearance [1], (2) breaking of colliding nuclei into pieces i.e. multi-fragmentation [2,3], (3) sub-threshold particle production [4] and (4) formation of hot and dense nuclear matter [5]. At high excitation energy, the colliding nuclei may break-up into several small and intermediate size fragments along with large number of nucleons that are also emitted. This is known as multi-fragmentation. The multi-fragmentation is the complex phenomena in nature which depends crucially on the incident energy of the projectile and on the geometry of the reaction [6]. At very low excitation energies, the excitation energy deposited in the system is too small to allow the break up of the nuclei into fragments. With the increase in the incident energy, the nuclei, after collision, can break up into dozens of fragments consisting of light, medium and heavy fragments. This phenomena was observed with the help of accelerators by Perfilov *et al.* and Lozkin *et al.* [7,8]. After 1982, Jakobsson *et al.* [9] observed a multiple emission of fragments of medium mass known as intermediate mass fragments (IMF's) in emulsion irradiation by the carbon beam of 250 MeV/nucleon at Berkeley BEVALAC. This scenario of multi-fragmentation was discussed in 1983 by Siemens [10]. Actually, the nuclear multi-fragmentation was discovered through cosmic rays accompanying the collisions of relativistic protons with targets and following the emission of slow fragments. These fragments were heavier than alpha particles but lighter than fission fragments. Also, the rise and fall of IMFs has also been established by Ogilvie *et al.* [11] through the collisions of Au particles with C, Al and Cu targets using ALADIN forward spectrometer at GSI, Darmstadt, with beam accelerated by SIS synchrotron.

The development of accelerators led to huge experimental data on multifragmentation. On theoretical front also, a large number of models have been proposed to study multi-fragmentation. These include statistical models and dynamical models. In the present paper, we aim to show the validity of quantum molecular dynamics model by confronting the calculations with the experimental data over wide range of energies.

## 2 The Formalism

### 2.1 Quantum Molecular Dynamics (QMD) model

We describe the time evolution of a heavy-ion reaction within the framework of Quantum Molecular Dynamics (QMD) model [12-15] which is based on a molecular dynamics picture. Here each nucleon is represented by a coherent state of the form

$$\phi_\alpha(x_1, t) = \left( \frac{2}{L\pi} \right)^{\frac{3}{4}} e^{-(x_1 - x_\alpha(t))^2} e^{ip_\alpha(x_1 - x_\alpha)} e^{-\frac{ip_\alpha^2 t}{2m}}. \quad (1)$$

where  $L$  is the Gaussian width of the particle. Thus, the wave function has two time dependent parameters  $x_\alpha$  and  $p_\alpha$ . The total  $n$ -body wave function is assumed to be a direct product of coherent states:

$$\phi = \phi_\alpha(x_1, x_\alpha, p_\alpha, t) \phi_\beta(x_2, x_\beta, p_\beta, t) \dots, \quad (2)$$

where antisymmetrization is neglected. One should, however, keep in the mind that the Pauli principle, which is very important at low incident energies, has been taken into account. The initial values of the parameters are chosen in a way that the ensemble ( $A_T + A_P$ ) nucleons give a proper density distribution as well as a proper momentum distribution of the projectile and target nuclei. The time evolution of the system is calculated using the generalized variational principle. We start out from the action

$$S = \int_{t_1}^{t_2} \mathcal{L}[\phi, \phi^*] d\tau, \quad (3)$$

with the Lagrange functional

$$\mathcal{L} = \left( \phi \left| i\hbar \frac{d}{dt} - H \right| \phi \right), \quad (4)$$

where the total time derivative includes the derivatives with respect to the parameters. The time evolution is obtained by the requirement that the action is stationary under the allowed variation of the wave function

$$\delta S = \delta \int_{t_1}^{t_2} \mathcal{L}[\phi, \phi^*] dt = 0. \quad (5)$$

If the true solution of the Schrödinger equation is contained in the restricted set of wave function  $\phi_\alpha(x_1, x_\alpha, p_\alpha)$ , this variation of the action gives the exact solution of the

Schrödinger equation. If the parameter space is too restricted, we obtain that wave function in the restricted parameter space which comes close to the solution of the Schrödinger equation. Performing the variation with the test wave function (2), we obtain for each parameter  $\lambda$  an Euler-Lagrange equation;

$$\frac{d}{dt} \frac{\partial \mathcal{L}}{\partial \dot{\lambda}} - \frac{\partial \mathcal{L}}{\partial \lambda} = 0. \quad (6)$$

For each coherent state and a Hamiltonian of the form,

$H = \sum_{\alpha} \left[ T_{\alpha} + \frac{1}{2} \sum_{\alpha\beta} V_{\alpha\beta} \right]$ , the Lagrangian and the Euler-Lagrange function can be easily calculated [15]

$$\mathcal{L} = \sum_{\alpha} \dot{\mathbf{x}}_{\alpha} \mathbf{p}_{\alpha} - \sum_{\beta} \langle V_{\alpha\beta} \rangle - \frac{3}{2Lm}, \quad (7)$$

$$\dot{\mathbf{x}}_{\alpha} = \frac{\mathbf{p}_{\alpha}}{m} + \nabla_{\mathbf{p}_{\alpha}} \sum_{\beta} \langle V_{\alpha\beta} \rangle, \quad (8)$$

$$\dot{\mathbf{p}}_{\alpha} = -\nabla_{\mathbf{x}_{\alpha}} \sum_{\beta} \langle V_{\alpha\beta} \rangle. \quad (9)$$

Thus, the variational approach has reduced the n-body Schrödinger equation to a set of 6n-different equations for the parameters which can be solved numerically. If one inspects the formalism carefully, one finds that the interaction potential which is actually the Brückner G-matrix can be divided into two parts: (i) a real part and (ii) an imaginary part. The real part of the potential acts like a potential whereas imaginary part is proportional to the cross section.

In the present model, interaction potential comprises of the following terms:

$$V_{\alpha\beta} = V_{loc}^2 + V_{loc}^3 + V_{Coul} + V_{Yuk}, \quad (10)$$

$V_{loc}$  is the Skyrme force whereas  $V_{Coul}$  and  $V_{Yuk}$  define, respectively, the Coulomb and Yukawa potentials. Yukawa term separates surface which also play role in low energy process like fusion and cluster radioactivity [16,17]. The expectation value of these potentials is calculated as

$$V_{loc}^2 = \int f_{\alpha}(\mathbf{p}_{\alpha}, \mathbf{r}_{\alpha}, t) f_{\beta}(\mathbf{p}_{\beta}, \mathbf{r}_{\beta}, t) V_I^{(2)}(\mathbf{r}_{\alpha}, \mathbf{r}_{\beta}) \times d^3\mathbf{r}_{\alpha} d^3\mathbf{r}_{\beta} d^3\mathbf{p}_{\alpha} d^3\mathbf{p}_{\beta}, \quad (11)$$

$$\begin{aligned}
V_{loc}^3 &= \int f_\alpha(\mathbf{p}_\alpha, \mathbf{r}_\alpha, t) f_\beta(\mathbf{p}_\beta, \mathbf{r}_\beta, t) f_\gamma(\mathbf{p}_\gamma, \mathbf{r}_\gamma, t) \\
&\quad \times V_I^{(3)}(\mathbf{r}_\alpha, \mathbf{r}_\beta, \mathbf{r}_\gamma) d^3\mathbf{r}_\alpha d^3\mathbf{r}_\beta d^3\mathbf{r}_\gamma \\
&\quad \times d^3\mathbf{p}_\alpha d^3\mathbf{p}_\beta d^3\mathbf{p}_\gamma.
\end{aligned} \tag{12}$$

where  $f_\alpha(\mathbf{p}_\alpha, \mathbf{r}_\alpha, t)$  is the Wigner density which corresponds to the wave functions (eq. 2).

If we deal with the local Skyrme force only, we get

$$V^{Skyrme} = \sum_{\alpha=1}^{A_T+A_P} \left[ \frac{A}{2} \sum_{\beta=1} \left( \frac{\tilde{\rho}_{\alpha\beta}}{\rho_0} \right) + \frac{B}{C+1} \sum_{\beta \neq \alpha} \left( \frac{\tilde{\rho}_{\alpha\beta}}{\rho_0} \right)^C \right]. \tag{13}$$

Here A, B and C are the Skyrme parameters which are defined according to the ground state properties of a nucleus. Different values of C lead to different equations of state. A larger value of C (= 380 MeV) is often dubbed as stiff equation of state. The finite range Yukawa ( $V_{Yuk}$ ) and effective Coulomb potential ( $V_{Coul}$ ) read as:

$$V_{Yuk} = \sum_{j,i \neq j} t_3 \frac{\exp\{-|\mathbf{r}_i - \mathbf{r}_j|\}/\mu}{|\mathbf{r}_i - \mathbf{r}_j|/\mu}, \tag{14}$$

$$V_{Coul} = \sum_{j,i \neq j} \frac{Z_{eff}^2 e^2}{|\mathbf{r}_i - \mathbf{r}_j|}. \tag{15}$$

The Yukawa interaction (with  $t_3 = -6.66$  MeV and  $\mu = 1.5$  fm) is essential for the surface effects. Also, the relativistic effect does not play role in low incident energy of present interest [18].

The phase space of the nucleons is stored at several time steps. The QMD model does not give any information about the fragments observed at the final stage of the reaction. In order to construct fragments from the present phase-space, one needs the clusterization algorithms. So, to construct fragments, we use Minimum Spanning Tree (MST) method.

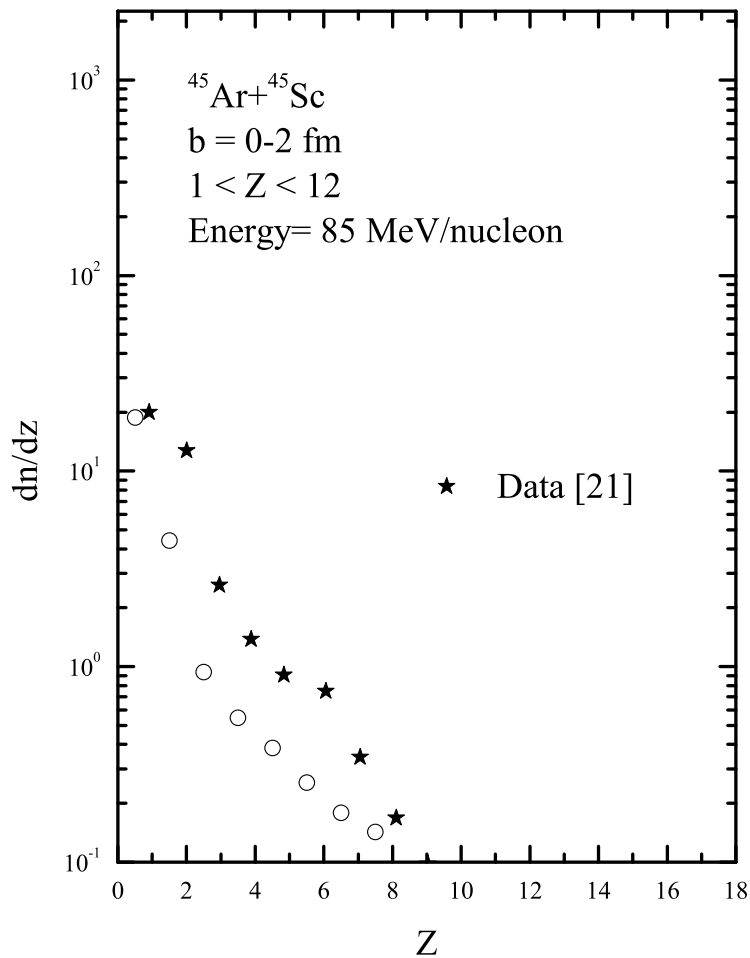


Figure 1: The charge distribution ( $dn/dz$ ) for the central collision of  $^{40}\text{Ar} + ^{45}\text{Sc}$  at an incident energy of 85 MeV/nucleon. The experimental data has been taken by the Ref. [21].

### 3 Minimum spanning tree (MST) method

The widely used clusterization algorithm is the Minimum Spanning Tree (MST) method [19]. In MST method, two nucleons are allowed to share the same fragment if their centroids are closer

than a distance  $r_{min}$ ,

$$|\mathbf{r}_i - \mathbf{r}_j| \leq r_{min}. \quad (16)$$

where  $\mathbf{r}_i$  and  $\mathbf{r}_j$  are the spatial positions of both nucleons. The value of  $r_{min}$  can vary between 2-4 fm. This method gives a big fragment at high density which splits into several light and medium mass fragments after several hundred fm/c. This procedure gives same fragment pattern for times later than 200 fm/c, but cannot be used for earlier times.

We simulate thousand events for the reactions of  $^{40}\text{Ar} + ^{45}\text{Sc}$  (at 85 and 115 MeV/nucleon),  $^{197}\text{Au} + ^{197}\text{Au}$  ( at 150 MeV/nucleon) and  $^{129}\text{Xe} + ^{119}\text{Sn}$  (at 25, 50 MeV/nucleon). The impact parameters have been guided by the corresponding experimental data. We use a soft equation of state along with standard energy-dependent nucleon-nucleon Cugnon cross-section. The details of the cross-section has been found in Ref. In fig. 1, we display the reaction of  $^{40}\text{Ar} + ^{45}\text{Sc}$  at central collision at an incident energy of 85 MeV/nucleon. Here, we display the charge distribution (open circles) for this reaction. The figure shows a linear decrease in the value of charge distribution ( $dn/dz$ ) with the charge. This negative slope of charge distribution indicates a gradual transition from the spectator matter to the disassembly of the system.

In the figure 2, we display the charge distribution for the reaction of  $^{40}\text{Ar} + ^{45}\text{Sc}$  at central collision at an incident energy of 115 MeV/nucleon. Here also, a decrease in the value of charge distribution is observed. Also, when the beam energy is increased from 85 MeV/nucleon to 115 MeV/nucleon, the slope is still steeper indicates the total disassembly of the matter. When we compare our theoretical results with experimental data, we see that our theoretical calculations matches well with the experimental data at both the energies. This experimental data are taken with Michigan State University (MSU) FOPI array [20,21] at the National Superconducting Cyclotron Laboratory (NSCL) using beams from K1200 Cyclotron. The FOPI array consists of a main ball of 170 phoswich counters covering angles from 23 degrees to 157 degrees.

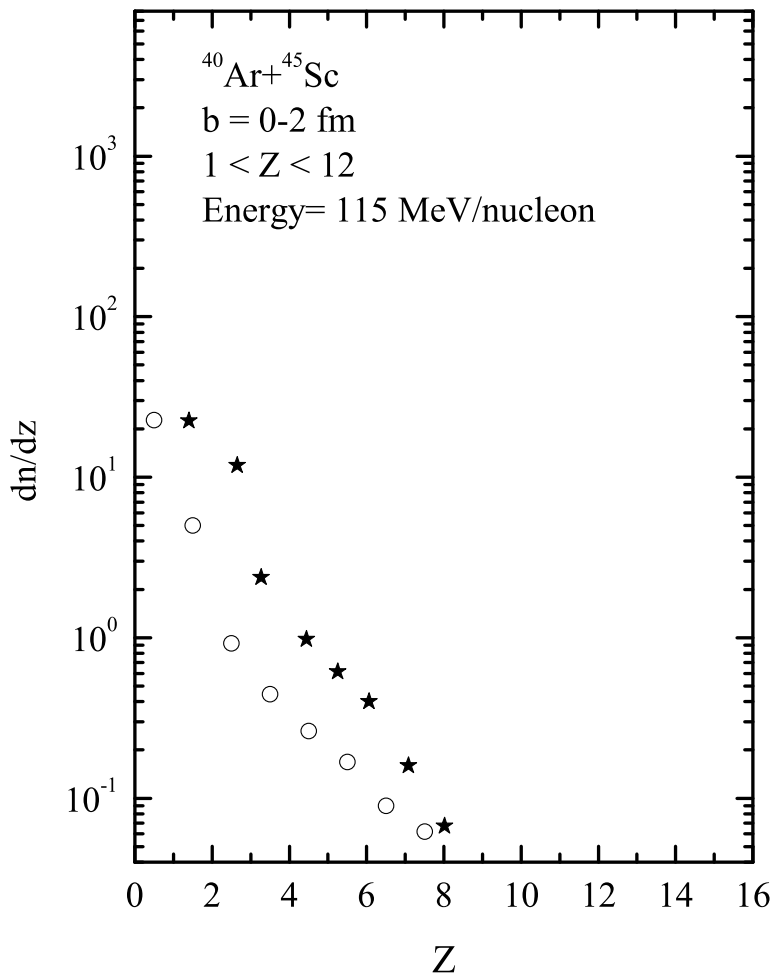


Figure 2: Same as figure 1, but at an incident energy of 115 MeV/nucleon. The experimental data has been taken by the Ref. [21].

In fig. 3, we display the results for the central collisions of  $^{197}\text{Au} + ^{197}\text{Au}$  collisions. This reaction was measured at the incident energy of  $E=150 \text{ MeV/nucleon}$ . Also, the condition of rapidity cut is applied so that there may be the covering of only those particles which are emitted

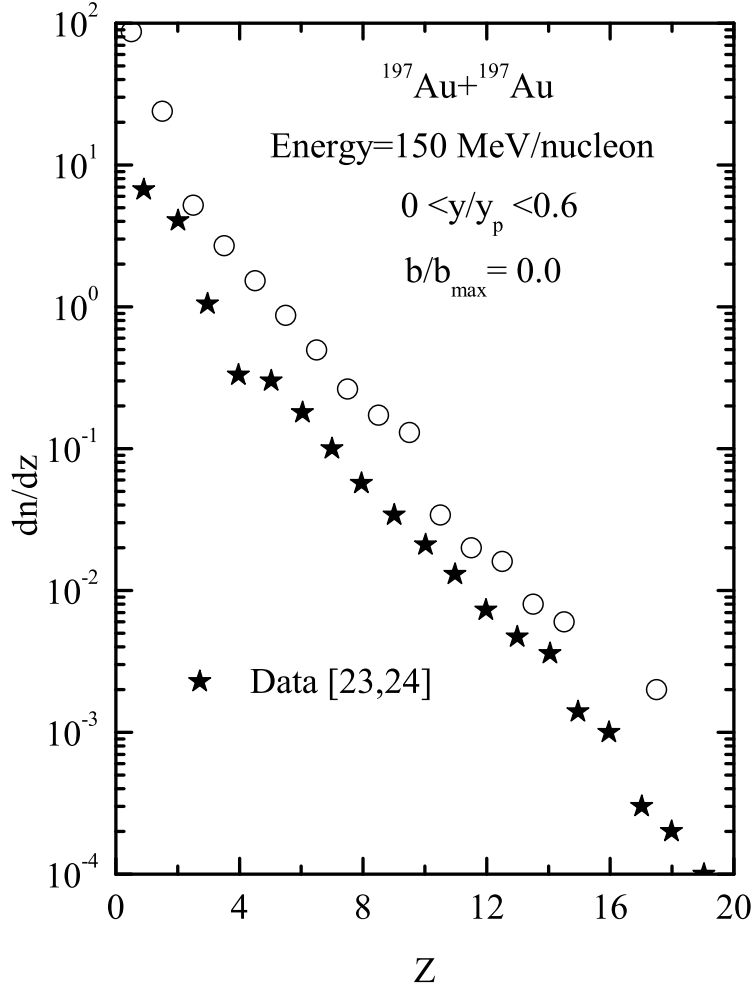


Figure 3: The multiplicity distribution ( $dn/dz$ ) of fragments measured for  $^{197}\text{Au} + ^{197}\text{Au}$  reaction at 150 MeV/nucleon having central collisions. The experimental data has been taken by the Ref. [23,24].

from the most violent reactions. This cut also removes the spectator particles i.e. only those particles are taken which took part in the reaction.

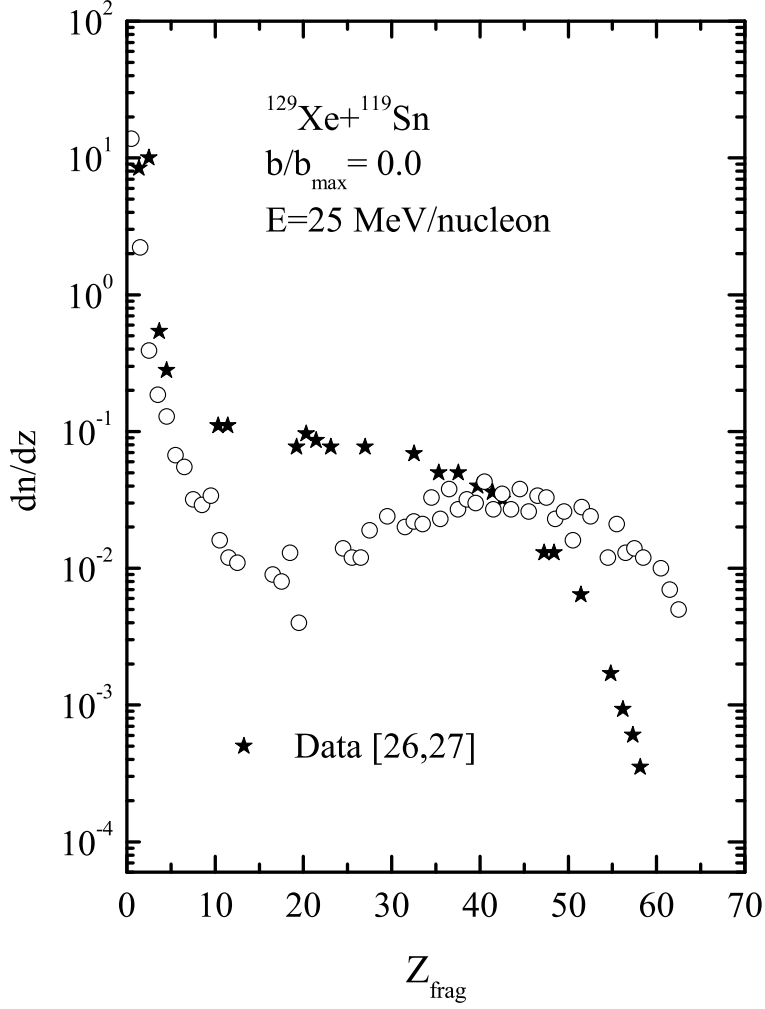


Figure 4: The charge distribution for central collisions of  $^{129}\text{Xe} + ^{119}\text{Sn}$  at bombarding energy of 25 MeV/nucleon. The experimental data has been taken by the Ref. [26,27].

In the figure, we again see a decrease in the value of charge distribution ( $dn/dz$ ) with the increase in charge. The reason is same as mentioned earlier in the description of figure 1. In the figure, the open circles show our theoretical calculations. When we compare our theoretical

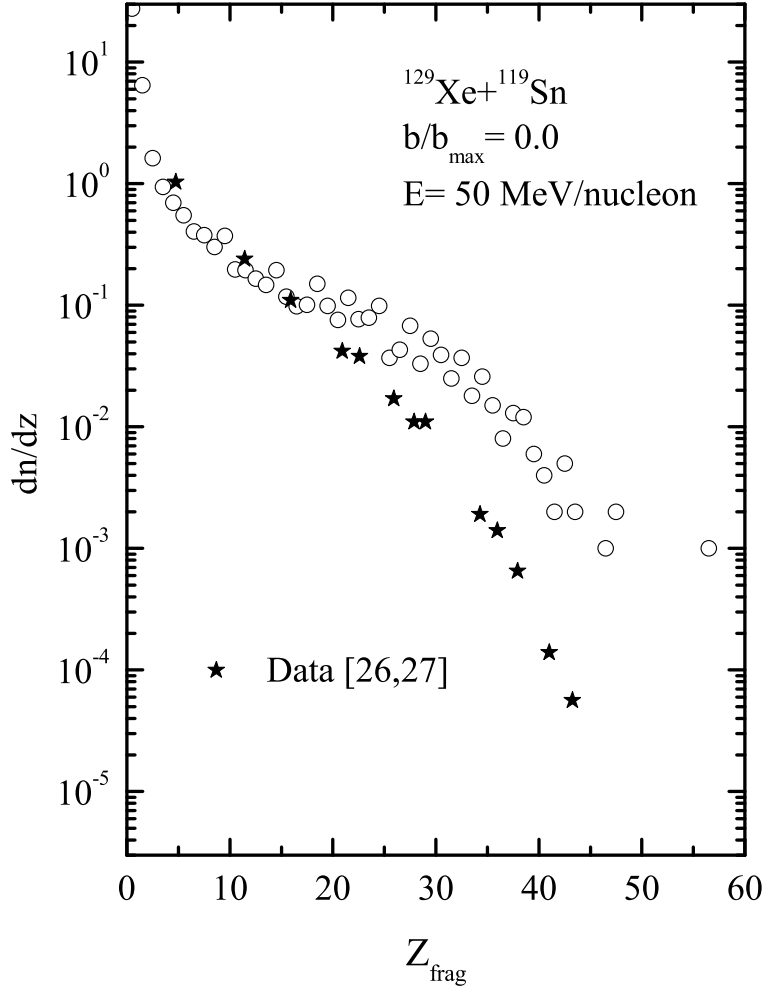


Figure 5: Same as Figure 4, but at incident energy of  $E = 50 \text{ MeV/nucleon}$ . The experimental data has been taken by the Ref. [26,27].

calculations with the experimental data, it matches well with each other. These experimental data are taken with the phase 1 set up of FOPI facility. The Au ion beam was delivered by the rapid-cycling synchrotron SIS, Darmstadt [22-24].

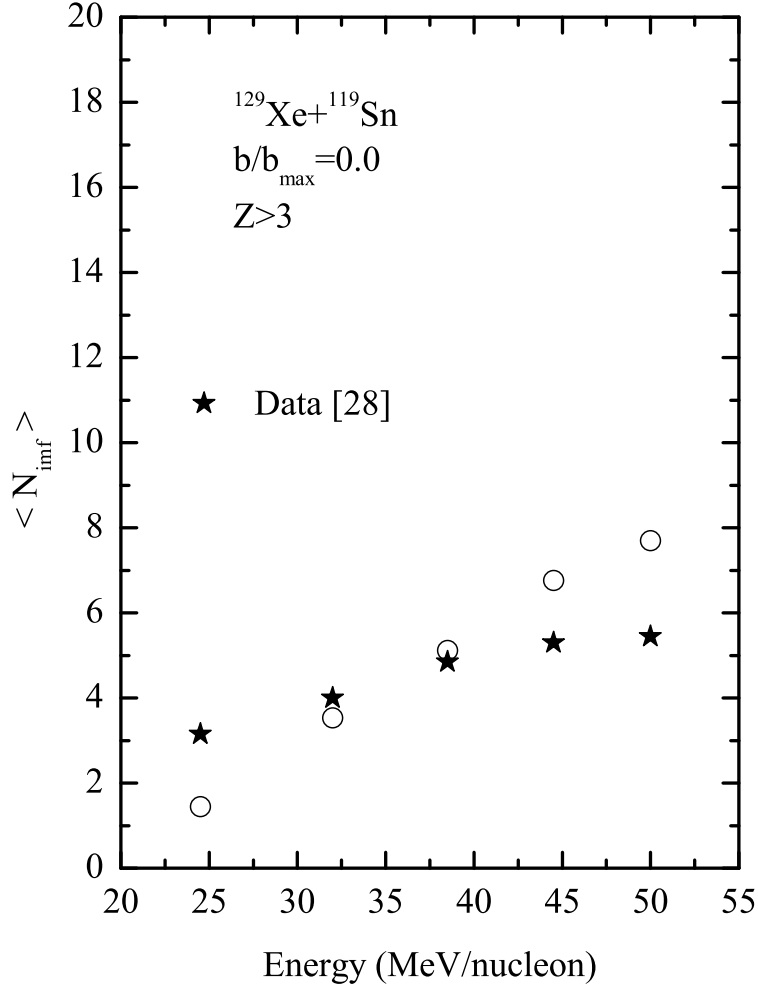


Figure 6: The IMF multiplicity versus beam energy is shown for central collision in the reaction of  $^{129}\text{Xe} + ^{119}\text{Sn}$ . The experimental data has been taken by the Ref. [28].

In fig. 4, we display the central collisions ( $b/b_{\text{max}}=0.0$ ) of  $^{129}\text{Xe} + ^{119}\text{Sn}$  at bombarding energy of  $E=25$  MeV/nucleon. Open circles shows our theoretical calculations done by the MST approach. In compare to previous results, we see now two separate zones. First, a negative

slope for light fragments and 'u' shape for heavy fragments. This indicates that at low energy, reaction produces excited compound system, thus cool down with the emission of free nucleons. Nearly, no intermediate mass fragment is seen in the reaction.

In figure 5, we again display the central collisions ( $b/b_{max}=0.0$ ) of  $^{129}\text{Xe} + ^{119}\text{Sn}$  at bombarding energy of  $E= 50$  MeV/nucleon. We again see a similar steepening of charge distribution with the charge. When we compare our theoretical calculations with the experimental data taken by the INDRA at the GANIL and GSI accelerator [25-27], they are in good agreement with each other.

In figure 6, we display the reaction of  $^{129}\text{Xe} + ^{119}\text{Sn}$  reaction for central collisions. We take only those particles with  $Z_i \geq 3$ . In the figure, we have seen the variation of number of intermediate mass fragments with the increase in the beam energy. At low energy i.e. 25 MeV/nucleon, number of IMFs produced is less because we have mainly the heavy fragment and free nucleons. Also, there is more time for the reaction to take place at low energy as compared to high energy. But with the increase in energy, there is increase in IMFs as shown in the figure. When our theoretical calculations are matched with the experimental data taken during the fragmentation studies performed with FOPI detector [28], they are in good agreement.

## Summary

We studied the different symmetric and asymmetric reactions mainly for central collisions with different range of energies. We observed the steepening of charge distribution with the increase in charge. Also, we observed that number of IMFs increases with the increase in beam energy. Our calculations showed good agreement with the data at all the energies.

## References

- [1] G. D. Westfall *et al.*, Phys. Rev. Lett. **71**, 1986 (1993); D. J. Magestro, W. R. Bauer and G. D. Westfall, Phys. Rev. C **62**, 041603(R) (2000); S. Kumar, M. K. Sharma, R. K. Puri, K. P. Singh and I. M. Govil, *ibid.*, **58**, 3494 (1998); A. D. Sood and R. K. Puri, *ibid.* **70**, 034611 (2004); **69**, 054612 (2004); **79**, 064618 (2009); A. Sood *et al.*, Eur. Phys. J **30**, 571 (2006); Phys. Lett. B **594**, 260 (2004); A. D. Sood and R. K. Puri, *ibid.* **73**, 067602 (2006).
- [2] M. B. Tsang *et al.*, Phys. Rev. C **53**, 1959 (1996); Andronic *et al.*, Nucl. Phys. A **679**, 765 (2001); S. Kumar, R. K. Puri and J. Aichelin, Phys. Rev. C **58**, 1618 (1998); J. Singh, S. Kumar and R. K. Puri, *ibid.*, **62**, 044617 (2000); S. Kumar, S. Kumar and R. K. Puri, *ibid.*, **78**, 064602 (2008); Y. K. Vermani, S. Goyal and R. K. Puri, Phys. Rev. C **79**, 064613 (2009); Y. Vermani *et al.*, Eur. Phys. Lett. **85**, 62001 (2009); Nucl. Phys. A **847**, 243 (2010).
- [3] G. Lehaut *et al.*, Phys. Rev. Lett. **104**, 232701 (2010); R. K. Puri and R. K. Gupta, J. Phys. G **18**, 903 (1992); S. S. Malik *et al.*, Pramana- J. Phys. **39**, 1992 (1989); R. K. Gupta, S. Singh, R. K. Puri and W. Scheid, Phys. Rev. C **47**, 561 (1993); R. K. Gupta *et al.*, J. Phys. G **18**, 1533 (1992).
- [4] S. W. Huang *et al.*, Phys. Lett. B **298**, 41 (1993); Prog. Nucl. Part. Phys. **30**, 105 (1993); G. Batko *et al.*, J. Phys. G **20**, 461 (1994).
- [5] D. T. Khoa *et al.*, Nucl. Phys. A **548**, 102 (1992); R. K. Puri *et al.*, *ibid.* **575**, 733 (1994); C. Fucks *et al.*, J. Phys. G. **22**, 131 (1996).
- [6] G. F. Peaslee *et al.*, Phys. Rev. C **49**, R2271 (1994); A. Schuettauf *et al.*, Nucl. Phys. A

- 607**, 457 (1996); K. Hagel *et al.*, Phys. Rev. Lett. **68**, 2141 (1992); N.T.B.Stone *et al.*, *ibid.* **78**, 2084 (1997); M. Bagemann-Blaich *et al.*, Phys. Rev. C **48**, 610 (1993); J. Hubble *et al.*, *ibid.* **46**, R1577 (1992); J. Hubble *et al.*, Z. Phys. A **340**, 263 (1991).
- [7] O. V. Lozkin and N. A. Perfilov, Zh. Eksp. Teor. Fiz. **31**, 913 (1956) [Sol. Phys. JETP 4, 790 (1956)].
- [8] N. A. Perfilov, O. V. Lozkin, and V. P. Shamov, Usp. Fiz Nauk **38**, 345 (1960) [Sov. Phys. Usp. **3**, 1 (1960)].
- [9] B. Jakobsson *et al.*, Z. Phys. A **307**, 293 (1982).
- [10] P. J. Siemens, Nature (London) **305**, 410 (1983).
- [11] C. A. Ogilvie *et al.*, Phys. Rev. Lett. **67**,1214 (1991).
- [12] R. K. Puri, C. Hartnack, and J. Aichelin, Phys. Rev. C **54**, R28 (1996); R. K. Puri and J. Aichelin, J. Comput. Phys. **162**, 245 (2000); Y. K. Vermani and R. K. Puri, Europhys. Lett. **85**, 62001 (2009); Y. K. Vermani, J. K. Dhawan, S. Goyal, R. K. Puri and J. Aichelin, J. Phys. G: Nucl. Part. Phys. **37**, 015105 (2010); S. Kumar, S. Kumar, and R. K. Puri, Phys. Rev. C **78**, 064602 (2008).
- [13] S. Kumar, M. K. Sharma, and R. K. Puri, Phys. Rev. C **58**, 3494 (1998); E. Lehmann *et al.*, Z. Phys. A **355**, 55 (1996); A. D. Sood and R. K. Puri, Phys. Rev. C **79**, 064618 (2009); A. D. Sood and R. K. Puri, Phys. Rev. C **70**, 034611 (2004); S. Kumar, S. Kumar, and R. K. Puri, Phys. Rev. C **81**, 014611 (2010); S. Kumar, S. Kumar, and R. K. Puri, Phys. Rev. C **81**, 014601 (2010); E. Lehmann *et al.*, Prog. Part. Nucl. Phys. **30**, 219 (1993); E. Lehmann *et al.*, Phys. Rev. C **51**, 2113 (1995).
- [14] J. Singh, S. Kumar, and R. K. Puri, Phys. Rev. C **62**, 044617 (2000); G. Batko *et al.*, J.

- Phys. G: Nucl. Part. Phys. **20**, 461 (1994); S. W. Huang *et al.*, Prog. Part. Nucl. Phys. **30**, 105 (1993); R. K. Puri *et al.*, Nucl. Phys. A **575**, 733 (1994); C. Fuchs *et al.*, J. Phys. G: Nucl. Part. Phys. **22**, 131 (1996).
- [15] J. Aichelin, Phys. Rep. **202**, 233 (1991).
- [16] R. K. Puri and R. K. Gupta, Phys. Rev. C **45**, 1837 (1992); R. K. Puri, M. K. Sharma, and R. K. Gupta, Eur. Phys. J A **3**, 277 (1998); I. Dutt and R. K. Puri, Phys. Rev. C **81**, 047601 (2010); *ibid.* C **81**, 044615 (2010); *ibid.* C **81**, 64609 (2010); *ibid.* C **81**, 64608 (2010); R. K. Puri and N. K. Dhiman, Eur. Phys. J A **23**, 429 (2005).
- [17] S. S. Malik *et al.*, Pram. J. Phys. **32**, 419 (1989); R. K. Puri, S. S. Malik, and R. K. Gupta, Europhys. Lett. **9**, 767 (1989); R. K. Puri and R. K. Gupta, J. Phys. G: Nucl. Part. Phys. **18**, 903 (1992); R. K. Gupta *et al.*, J. Phys. G: Nucl. Part. Phys. **26**, L23 (2000).
- [18] E. Lehmann *et al.*, Phys. Rev. C **51**, 2113 (1995); *ibid.*, Prog. Part. Nucl. Phys. **30** 219 (1993).
- [19] J. Singh and R. K. Puri, J. Phys. G: Nucl. Part. Phys. **27**, 2091 (2001); S. Kumar, and R. K. Puri, Phys. Rev. C **58**, 2858 (1998).
- [20] T. Li, W. Bauer, D. Craig *et al.*, Phys. Rev. Lett. **70**, 1924 (1993).
- [21] G. D. Westfall, J. E. Yurkon, J. van der Plicht, Z. M. Koenig, B. V. Jacak, R. Fox, G. M. Crawley, M. R. Maier, B. E. Hasselquist, R. S. Tickle and D. Horn, Nucl. Instrum. Methods Phys. Res., Sect. A **238**, 347 (1985).
- [22] C. Kuhn, J. Konopka, J. P. Coffin *et al.*, Phys. Rev. C **48**, 1232 (1993).
- [23] J. P. Coffin for the FOPI Collaboration at GSI, Int. J. Mod. Phys. E : Reports on Nucl. Phys., Vol. 1 No. 4, 739 (1992).

- [24] A. Gobbi and the FOPI Collaboration at GSI, Nucl. Instrum. Methods A **324**, 156 (1993).
- [25] J. D. Frankland, R. Bougault, A. Chbihi *et al.*, Contribution to International Workshop on multifragmentation and related topics (IWM2001), LNS Catania, Italy, Nov. 28- Dec. 1, 2001.
- [26] E. Plagnol, *et al.* (INDRA collaboration), Phys. Rev. C **61**, 014606 (1999).
- [27] S. Hudan, Doctorat de 1' Universite de Caen, GANIL T **01 07** (2001).
- [28] B. Borderie, M. F. Rivet, Progress in Particle and Nuclear Physics **61**, 551(2008).